



Optics Letters

Mid-infrared frequency comb generation via cascaded quadratic nonlinearities in quasi-phase-matched waveguides

ABIJITH S. KOWLIGY,^{1,*} ALEX LIND,^{1,2} DANIEL D. HICKSTEIN,¹ DAVID R. CARLSON,¹ HENRY TIMMERS,¹ NIMA NADER,³ FLAVIO C. CRUZ,^{1,4} GABRIEL YCAS,³ SCOTT B. PAPP,¹ AND SCOTT A. DIDDAMS^{1,2}

¹Time and Frequency Division, National Institute of Standards and Technology, 325 Broadway, Boulder, Colorado 80305, USA

²Department of Physics, University of Colorado, Boulder, Colorado 80305, USA

³Applied Physics Division, National Institute of Standards and Technology, 325 Broadway, Boulder, Colorado 80305, USA

⁴Instituto de Física Gleb Wataghin, Universidade Estadual de Campinas, Campinas, SP, 13083-859, Brazil

*Corresponding author: abijith.kowligy@gmail.com

Received 25 January 2018; revised 7 March 2018; accepted 8 March 2018; posted 8 March 2018 (Doc. ID 320558); published 5 April 2018

We experimentally demonstrate a simple configuration for mid-infrared (MIR) frequency comb generation in quasi-phase-matched lithium niobate waveguides using the cascaded- $\chi^{(2)}$ nonlinearity. With nanojoule-scale pulses from an Er:fiber laser, we observe octave-spanning supercontinuum in the near-infrared with dispersive wave generation in the 2.5–3 μm region and intrapulse difference frequency generation in the 4–5 μm region. By engineering the quasi-phase-matched grating profiles, tunable, narrowband MIR and broadband MIR spectra are both observed in this geometry. Finally, we perform numerical modeling using a nonlinear envelope equation, which shows good quantitative agreement with the experiment—and can be used to inform waveguide designs to tailor the MIR frequency combs. Our results identify a path to a simple single-branch approach to mid-infrared frequency comb generation in a compact platform using commercial Er:fiber technology. © 2018 Optical Society of America

OCIS codes: (190.0190) Nonlinear optics; (130.3060) Infrared; (320.6629) Supercontinuum generation.

<https://doi.org/10.1364/OL.43.001678>

Mid-infrared (3–25 μm) frequency combs are desirable for many multidisciplinary scientific goals including precision spectroscopy in the molecular fingerprint region [1], referencing quantum cascade lasers (QCL) [2], probing fundamental symmetries in physics [3], and novel imaging techniques [4]. For certain applications such as dual-comb spectroscopy (DCS) [5] and absolute frequency metrology [6], compact and chip-scale geometries are also desirable. In the near-infrared (NIR), frequency combs have seen extensive research and development due to the robust and commercially available erbium-, ytterbium-, and thulium-doped gain fiber, whereas the MIR has been less explored [7,8]. Nascent technologies such as MIR QCL frequency combs have also been demonstrated [9]. In contrast,

frequency conversion to the MIR using robust, stable NIR frequency combs in quadratic ($\chi^{(2)}$) and cubic ($\chi^{(3)}$) media has been appealing due to the availability of high-power amplifiers in the NIR region and widely transparent nonlinear optical materials. Such nonlinear techniques include parametric oscillation in $\chi^{(2)}$ and $\chi^{(3)}$ optical cavities [10–12], difference frequency generation (DFG) [13,14], and supercontinuum generation (SCG) [15].

DFG, in particular, has been the workhorse of many experiments utilizing MIR frequency combs. Owing to the inherent offset-frequency subtraction in the DFG process, comb stabilization is simplified—requiring only repetition rate stability [16]. However, conventional DFG experiments are difficult to miniaturize due to the requisite spatio-temporal alignment for the pump and the signal pulses [13,14], which typically requires alignment optics and mechanical delay stages. In contrast, SCG requires only a single pulse, but conversion efficiency to the MIR is limited [15].

In this Letter, we experimentally demonstrate a simplified configuration for MIR frequency comb generation by combining spectral broadening and difference frequency generation in the same nonlinear optical waveguide. In particular, we utilize the nonlinear broadening due to the cascaded- $\chi^{(2)}$ [17,18] nonlinearity in a quasi-phase-matched (QPM) waveguide and intrapulse difference frequency mixing to generate MIR frequency combs. In the cascaded- $\chi^{(2)}$ process, the pump pulse undergoes strong intensity-dependent phase modulation induced by phase-mismatched second-harmonic generation (SHG) [18]. This results in an effective, self-defocusing cubic nonlinearity and leads to spectral broadening in the normal dispersion regime. Since the phase mismatch is controlled by the QPM grating profile, engineered quadratic and effective cubic nonlinear interactions are possible, finding both quantum and classical applications in squeezed light generation [19], all-optical switching [20], femtosecond pulse generation [21], broadband SCG [22,23], and frequency comb stabilization [24,25]. In previous comb stabilization experiments, octave

spanning supercontinua in the NIR were observed in reverse-proton-exchanged PPLN waveguides using Yb: and Tm: fiber lasers [24,25], but relatively high pulse energies (>10 nJ) were required. In a previous Er: fiber-pumped experiment, the infrared wavelengths did not extend beyond 3 μm [24].

Using an Er: fiber laser pump, we demonstrate frequency combs in the 4–5 μm region in two configurations: (i) tunable, offset-free, narrowband mid-infrared light in 4-cm-long periodically poled waveguides and (ii) broadband MIR in chirped (aperiodically poled, aPP) waveguides. In the cascaded- $\chi^{(2)}$ -driven SCG, we also observe the generation of dispersive waves in the 2.5–3 μm region. Finally, we verify the utility of such broadband combs in a proof-of-principle multi-heterodyne experiment using two offset-free combs in the 4.8- μm region.

We use a turnkey Er: fiber laser (100 MHz repetition rate, [26]) to pump the waveguides [Fig. 1(a)]. The laser output is amplified with a nonlinear Er: fiber amplifier to yield 80-fs (FWHM), 2-nJ pulses. Aspheric lenses are used to couple light in and out of the 4-cm-long PPLN waveguide, and we measure a total insertion loss of 3 dB, including the coupling loss, Fresnel reflections off the uncoated facets, and linear scattering loss. The output spectra are measured using a combination of grating- and Fourier-transform spectrometers. The waveguide chip contains 20 waveguides with grating periods spanning 25.8–29.6 μm in 0.2 μm increments. The waveguides are PPLN ridges on a lithium tantalate substrate [27] and have cross section dimensions of 12.6 $\mu\text{m} \times 12 \mu\text{m}$ [Fig. 1(b)].

With these waveguides, we observe cascaded- $\chi^{(2)}$ -driven SCG in the NIR including dispersive wave generation in the 2.5–3 μm region due to the zero-crossing in the group velocity dispersion (GVD, $\lambda_{\text{ZDW}} = 1.87 \mu\text{m}$). The GVD includes the contribution of the waveguide dispersion, which blue shifts λ_{ZDW} by 50 nm compared to bulk material ($\lambda_{\text{ZDW}} = 1.92 \mu\text{m}$). In this process, the pump pulse undergoes soliton fission, providing broadening in the spectral domain and temporal compression in the time domain [28,29].

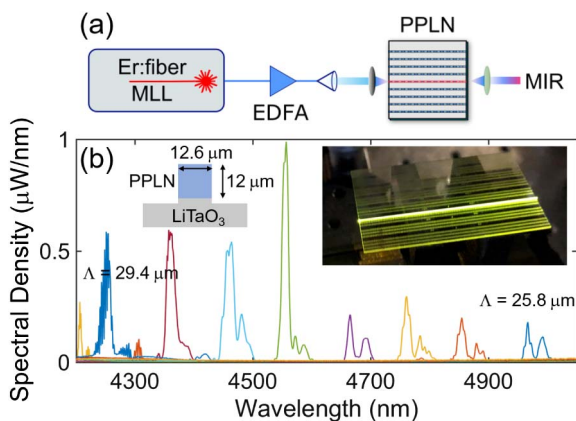


Fig. 1. (a) Femtosecond pulses from a 1.5 μm Er: fiber mode-locked laser (MLL) are amplified with an erbium-doped fiber amplifier (EDFA), and focused into periodically poled lithium niobate (PPLN) waveguides. The generated MIR light is sent to a spectrometer or photodetector. (b) DFG spectra from the waveguide chip as the poling periods are tuned from $\Lambda = 25.8 \mu\text{m}$ to $\Lambda = 29.4 \mu\text{m}$. (Inset left): the small cross section of the PPLN waveguide provides strong optical confinement and high intensity. (Inset right): the waveguide glows with visible light as a result of sum-frequency generation.

Simultaneously, intrapulse DFG occurs in the waveguide, resulting in MIR light. As the grating period is changed, the MIR is smoothly tuned from 4 to 5 μm [Fig. 2(a)]. Owing to the multimode waveguide, we also observed phase matching to higher order spatial modes that results in additional DFG peaks [Fig. 2(a)]. Spectrally filtering and imaging the MIR on a microbolometer-array camera confirmed the presence of other spatial modes. Stable alignment of the pump to the TM_{00} mode is maintained over several hours and monitored by imaging the output mode on a camera. The TM_{00} DFG power is on the order of 100 μW in each waveguide. The relatively long interaction length in the waveguide results in a narrow DFG phase-matching bandwidth, $\Delta\lambda_{\text{FWHM}} \approx 20 \text{ nm}$. We note that similar DFG has been observed in bulk PPLN crystals recently and termed as DFG resonant radiation [22].

We model the nonlinear optical dynamics in the waveguide for the TM_{00} mode using the single-mode nonlinear analytic envelope equation [22,30,31],

$$\begin{aligned} \frac{\partial A}{\partial z} + i\hat{D}A(z, t) &= i\left(1 + \frac{i}{\omega_0} \frac{\partial}{\partial t}\right) \times \left[\chi(z)(A^2 e^{-i\varphi(z, t)} + |A|^2 e^{i\varphi(z, t)}) \right. \\ &\quad \left. + \gamma \left(|A|^2 A + A \int dt' R(t, t') |A|^2(t') \right) \right], \end{aligned} \quad (1)$$

where $\hat{D} = \sum_{j=2} \frac{1}{j!} k_j (i \frac{\partial}{\partial t})^j$ is the dispersion operator, $\chi(z) = \chi^{(2)}(z) \omega_0^2 / 4\beta_0 c^2$, $\varphi(z, t) = \omega_0 t - (\beta_0 - \beta_1 \omega_0)z$, $\gamma = n_2 \omega_0 / c A_{\text{eff}}$ is the nonlinear Kerr parameter, and $R(t, t')$ is the Raman response function for lithium niobate [32]. For this Letter,

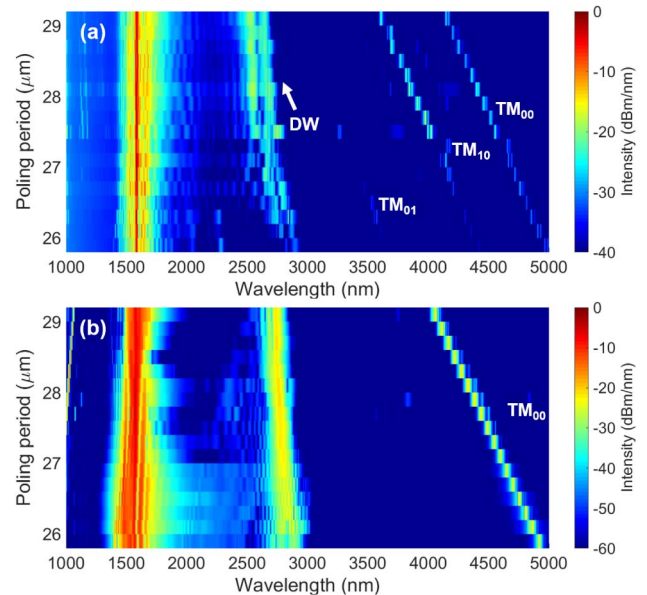


Fig. 2. (a) Experimental spectra for cascaded- $\chi^{(2)}$ spectral broadening and tunable, intrapulse DFG in 4-cm-long PPLN waveguides are shown as a function of grating period. Due to the multimode nature of the waveguide, the DFG also occurs in higher order spatial modes obeying their own phase-matching conditions and leads to additional discrete peaks in the mid-IR. The spectral broadening is also accompanied by dispersive wave (DW) generation in the 2.5–3 μm wavelength region. (b) The corresponding theoretical spectra for TM_{00} , generated using a single-mode nonlinear analytic envelope equation, showing good agreement with the experiment.

we assume $d_{\text{eff}} = 19 \text{ pm/V}$, $n_2 = 2.5 \times 10^{-16} \text{ cm}^2/\text{W}$, and the Raman fraction to be $f_R = 0.2$. For the $\chi^{(2)}$ nonlinearity, we take into account all the orders of the grating and use the full dispersion function, $k(\omega)$, calculated for the waveguides via COMSOL, which also yields an effective area, $A_{\text{eff}} = 75 \text{ }\mu\text{m}^2$, for the pump mode. By taking into account the quadratic and cubic nonlinearities of lithium niobate, the model reproduces the different spectra observed from the various waveguides [Fig. 2(b)].

We also study the propagation dynamics of a single waveguide ($\Lambda = 29.6 \text{ }\mu\text{m}$, Fig. 3). The observed SCG in the NIR has contributions from both the quadratic and cubic (Kerr) nonlinearities: the total cubic nonlinearity is the sum of positive n_2 from the Kerr nonlinearity and the negative, effective n_2 arising from the cascaded- $\chi^{(2)}$ effect, resulting in a net negative value. Compared to conventional SCG, where anomalous GVD ($\beta_2 < 0$) balances the positive n_2 to facilitate soliton formation and fission, the observed SCG occurs in the normal dispersion regime ($\beta_2 > 0$), balancing the negative n_2 . Temporal compression also occurs in the self-defocusing nonlinear dynamics [33] to yield few-cycle pulses, $\tau_{\text{FWHM}} \approx 13 \text{ fs}$, at the point of soliton fission [Fig. 3(b)]. Thus, one could engineer the grating profile and waveguide dimensions to tailor the output spectra using the cascaded- $\chi^{(2)}$ nonlinearity toward subnanjoule-scale, few-cycle pulses [33].

The ability to quasi-continuously tune the DFG across the first atmospheric window is valuable for applications such as targeted spectroscopy in molecules [34]. In other cases, such as dual-comb spectroscopy, broader MIR bandwidths enable spectroscopy of broadband absorbers while maintaining the frequency accuracy provided by the comb [5]. By employing chirped QPM grating profiles, such broadband MIR spectra can be obtained. Using aPPLN waveguides, we demonstrate the broadband DFG [Figs. 4(a) and 4(b)], which is well predicted by the numerical modeling [Eq. (1)].

We investigate two aPPLN waveguides, with cross sectional dimensions of $15 \text{ }\mu\text{m} \times 16 \text{ }\mu\text{m}$, simultaneously using two Er: fiber lasers for a dual-comb (or multiheterodyne) experiment. First, in a 10-mm-long waveguide (with a chirp in the grating from 33 to 29 μm), the DFG light is generated with $\Delta\lambda_{\text{FWHM}} = 150 \text{ nm}$ around 4.8 μm using a 40-fs, 1.5-nJ pump pulse

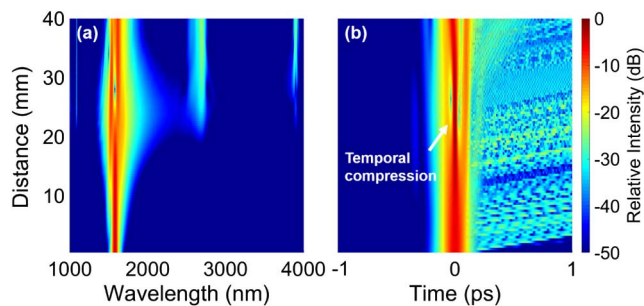


Fig. 3. (a) Spectral evolution as a function of distance in the 40-mm-long waveguide ($\Lambda = 29.2 \text{ }\mu\text{m}$). The soliton fission length is approximately 20 mm. Narrowband 1- μm light is generated due to phase-matched second-harmonic generation from the 2 μm region of the supercontinuum. (b) The temporal evolution of the pulse as a function of distance in the pump frame-of-reference. Temporal compression occurs in the time domain (minimum pulse duration, $\tau_{\text{FWHM}} = 13 \text{ fs}$). Group velocity walk-off is observed for the DFG, limiting conversion efficiency and bandwidth.

[Fig. 4(a)]. In a second 5-mm-long waveguide (with a chirp in the grating from 29 to 27 μm), a decade-spanning continuum (0.5–5 μm) is generated [Fig. 4(b)] using a few-cycle, 1.5-nJ pump pulse derived from an Er: fiber laser [35]. We note that similar broad spectra were also observed with an uncompressed, spectrally broad input to a PPLN waveguide [36]. A chalcogenide aspheric lens and a parabolic mirror are used as output couplers for the 10-mm-long and 5-mm-long waveguides, respectively.

For DCS experiments, highly coherent combs and milliwatt-scale optical powers are desirable. To demonstrate this utility of the MIR generated by the cascaded- $\chi^{(2)}$ process, we perform a proof-of-principle multiheterodyne experiment with the spectra in Figs. 4(a) and 4(b). The repetition rates of the two pump lasers are locked to a microwave frequency reference and offset by $\Delta f_{\text{rep}} = 50 \text{ Hz}$. The milliwatt-scale MIR spectra are spectrally filtered using a 4.5- μm long-pass filter and combined on a CaF_2 beam splitter. A liquid-nitrogen-cooled mercury-cadmium-telluride (HgCdTe)

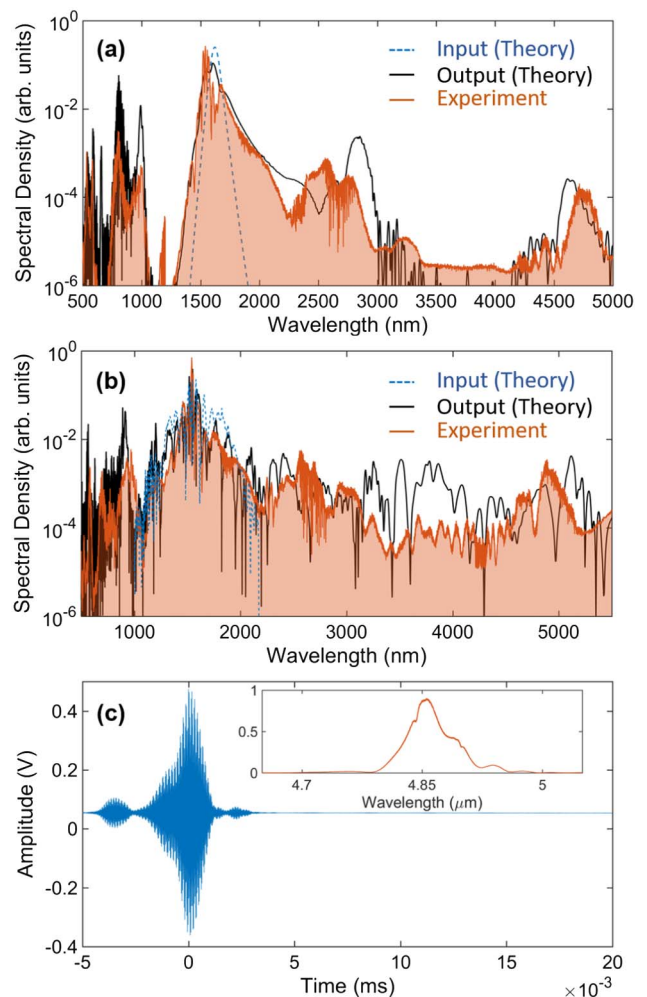


Fig. 4. (a), (b) Experimental and modeled spectra for (a) 10-mm-long aPPLN waveguide, yielding broadband light in the 4.8 μm region and (b) 0.5-cm-long aPPLN waveguide, showing a continuum across the 0.5–5 μm decade. (c) The center burst of the interferogram resulting from the multiheterodyne of the two combs in (a) and (b). (Inset): the dual-comb spectrum.

detector is used for photodetection. The time domain signal is measured over the window, $T = 1/\Delta f_{\text{rep}} = 20$ ms, with >350 signal-to-noise ratio (SNR) acquired by averaging 1024 interferograms [Fig. 4(c)]. The coherent MIR waveguide output enables high SNR and provides for 100 MHz resolution in the dual-comb spectrum [Fig. 4(c), inset]. The DCS bandwidth is limited by the 10-mm-device MIR spectrum but can be addressed by engineering the QPM grating [37].

In summary, we have demonstrated a robust and straightforward technique for mid-infrared frequency comb generation in the 4–5 μm band in QPM lithium niobate waveguides. Using the cascaded- $\chi^{(2)}$ nonlinearities, a single mode-locked Er:fiber laser is able to access the MIR wavelengths. By engineering the QPM grating profile, the mid-infrared spectra can be made narrowband or broadband. In addition, the DFG combs are offset-free and simplify comb stabilization. By using two such combs, we demonstrated stable multiheterodyne beating and presented an MIR dual-comb spectrum. We also modeled the nonlinear dynamics using a nonlinear envelope equation, which showed good agreement with the experimentally acquired spectra. This QPM-enabled engineering of quadratic and effective cubic nonlinear interactions allows for spectral engineering across multiple octaves—providing control over both the nonlinear strength and dispersion on a compact platform. Additionally, future work would benefit from more sophisticated dispersion engineering resulting from stronger optical confinement in waveguides and reduce the pump power threshold for these nonlinear processes. Such improvements could make this approach accessible to GHz repetition rate lasers—recently, a 250-MHz Er:fiber laser using only 600 pJ pump pulse energy showed similar MIR comb generation [38].

Funding. Defense Advanced Research Projects Agency (DARPA) (SCOUT); Air Force Office of Scientific Research (AFOSR) (FA9550-16-1-0016); National Institute of Standards and Technology (NIST); National Aeronautics and Space Administration (NASA); National Research Council.

Acknowledgment. The authors thank Daryl Spencer and Franklyn Quinlan for helpful comments and Dr. Yoshiki Nishida for providing the PPLN waveguide chips. This Letter is a contribution of the United States government and is not subject to copyright in the USA.

REFERENCES

1. A. Schliesser, N. Picque, and T. W. Hansch, *Nat. Photonics* **6**, 440 (2012).
2. K. Knabe, P. A. Williams, F. R. Giorgetta, M. B. Radunsky, C. M. Armacost, S. Crivello, and N. R. Newbury, *Opt. Express* **21**, 1020 (2013).
3. C. Stoeffler, B. Darquié, A. Shelkovich, C. Daussy, A. Amy-Klein, C. Chardonnet, L. Guy, J. Crassous, T. R. Huet, P. Souillard, and P. Asselin, *Phys. Chem. Chem. Phys.* **13**, 854 (2011).
4. M. A. Huber, M. Plankl, M. Eisele, R. E. Marvel, F. Sandner, T. Korn, C. Schüller, R. F. Haglund, R. Huber, and T. L. Cocker, *Nano Lett.* **16**, 1421 (2016).
5. I. Coddington, N. Newbury, and W. Swann, *Optica* **3**, 414 (2016).
6. P. Malara, P. Maddaloni, G. Gagliardi, and P. D. Natale, *Opt. Express* **16**, 8242 (2008).
7. T. Hu, S. D. Jackson, and D. D. Hudson, *Opt. Lett.* **40**, 4226 (2015).
8. S. Antipov, D. D. Hudson, A. Fuerbach, and S. D. Jackson, *Optica* **3**, 1373 (2016).
9. A. Hugi, G. Villares, S. Blaser, H. C. Liu, and J. Faist, *Nature* **492**, 229 (2012).
10. M. Vainio and L. Halonen, *Phys. Chem. Chem. Phys.* **18**, 4266 (2016).
11. C. Y. Wang, T. Herr, P. Del'Haye, A. Schliesser, J. Hofer, R. Holzwarth, T. W. Hänsch, N. Picqué, and T. J. Kippenberg, *Nat. Commun.* **4**, 2335 (2013).
12. M. Yu, Y. Okawachi, A. G. Griffith, M. Lipson, and A. L. Gaeta, "Modelocked mid-infrared frequency combs in a silicon microresonator," arXiv:1604.06501 [physics] (2016).
13. C. Erny, K. Moutzouris, J. Biegert, D. Kuhlke, F. Adler, A. Leitenstorfer, and U. Keller, *Opt. Lett.* **32**, 1138 (2007).
14. F. C. Cruz, D. L. Maser, T. Johnson, G. Ycas, A. Klose, F. R. Giorgetta, I. Coddington, and S. A. Diddams, *Opt. Express* **23**, 26814 (2015).
15. D. D. Hickstein, H. Jung, D. R. Carlson, A. Lind, I. Coddington, K. Srinivasan, G. G. Ycas, D. C. Cole, A. Kowligy, C. Fredrick, S. Droste, E. S. Lamb, N. R. Newbury, H. X. Tang, S. A. Diddams, and S. B. Papp, *Phys. Rev. Appl.* **8**, 014025 (2017).
16. A. Baltuška, T. Fuji, and T. Kobayashi, *Phys. Rev. Lett.* **88**, 133901 (2002).
17. G. I. Stegeman, D. J. Hagan, and L. Torner, *Opt. Quantum Electron.* **28**, 1691 (1996).
18. R. DeSalvo, D. J. Hagan, M. Sheik-Bahae, G. Stegeman, E. W. V. Stryland, and H. Vanherzeele, *Opt. Lett.* **17**, 28 (1992).
19. S. Youn, S.-K. Choi, P. Kumar, and R.-D. Li, *Opt. Lett.* **21**, 1597 (1996).
20. G. S. Kanter, P. Kumar, K. R. Parameswaran, and M. M. Fejer, *IEEE Photon. Technol. Lett.* **13**, 341 (2001).
21. F. Wise, L. Qian, and X. Liu, *J. Nonlinear Opt. Phys. Mater.* **11**, 317 (2002).
22. B. Zhou, X. Liu, H. Guo, X. Zeng, X. Chen, H. Chung, Y. Chen, and M. Bache, *Phys. Rev. Lett.* **118**, 143901 (2017).
23. H. Wang, A. Alismail, G. Barbiero, M. Wendl, and H. Fattahi, *Opt. Lett.* **42**, 2595 (2017).
24. C. Langrock, M. M. Fejer, I. Hartl, and M. E. Fermann, *Opt. Lett.* **32**, 2478 (2007).
25. C. R. Phillips, C. Langrock, J. S. Pelc, M. M. Fejer, J. Jiang, M. E. Fermann, and I. Hartl, *Opt. Lett.* **36**, 3912 (2011).
26. L. C. Sinclair, J.-D. Deschênes, L. Sonderhouse, W. C. Swann, I. H. Khader, E. Baumann, N. R. Newbury, and I. Coddington, *Rev. Sci. Instrum.* **86**, 081301 (2015).
27. Y. Nishida, H. Miyazawa, M. Asobe, O. Tadanaga, and H. Suzuki, *Electron. Lett.* **39**, 609 (2003).
28. J. M. Dudley, G. Genty, and S. Coen, *Rev. Mod. Phys.* **78**, 1135 (2006).
29. B. Zhou and M. Bache, *Opt. Lett.* **40**, 4257 (2015).
30. C. R. Phillips, C. Langrock, J. S. Pelc, M. M. Fejer, I. Hartl, and M. E. Fermann, *Opt. Express* **19**, 18754 (2011).
31. M. Conforti, F. Baronio, and C. De Angelis, *Phys. Rev. A* **81**, 053841 (2010).
32. M. Bache and R. Schiek, "Review of measurements of Kerr nonlinearities in lithium niobate: the role of the delayed Raman response," arXiv:1211.1721 (2012).
33. J. Moses and F. W. Wise, *Opt. Lett.* **31**, 1881 (2006).
34. C.-H. Chang and D. J. Nesbitt, *J. Chem. Phys.* **145**, 044304 (2016).
35. H. Timmers, A. Kowligy, A. Lind, N. Nader, G. Ycas, P. G. Schunemann, S. Papp, and S. Diddams, *Nonlinear Optics* (Optical Society of America, 2017), paper NTH3A.4.
36. K. Iwakuni, S. Okubo, O. Tadanaga, H. Inaba, A. Onae, F.-L. Hong, and H. Sasada, *Opt. Lett.* **41**, 3980 (2016).
37. C. R. Phillips and M. M. Fejer, *Opt. Lett.* **35**, 3093 (2010).
38. A. Lind, A. S. Kowligy, D. D. Hickstein, D. Carlson, N. Nader, H. Timmers, E. Lamb, G. Ycas, S. Papp, and S. Diddams, *Frontiers in Optics* (Optical Society of America, 2017), paper FTu4D.4.